XII International Conference on Computational Plasticity. Fundamentals and Applications
COMPLAS XII
E. Oñate, D.R.J. Owen, D. Peric and B. Suárez (Eds)

MICRO-MODELING OF STACK BOND MASONRY IN COMPRESSION USING A PLASTICITY LAW

ANASTASIOS DROUGKAS*, PERE ROCA* AND CLIMENT MOLINS*

* Departament d'Enginyeria de la Construcció
Universitat Politècnica de Catalunya
Campus Diagonal Nord, Building C1, Jordi Girona 1-3 UPC, 08034 Barcelona, Spain
e-mail: anastasios.drougkas@upc.edu

Key words: Micro-modeling, Masonry, Compressive Strength, Young's Modulus

Abstract. A set of experimental tests to determine the compressive strength of masonry stack prisms has been numerically simulated using a combined plasticity-smeared crack constitutive law employed in three-dimensional analysis.

Supported by an experimental campaign for the mechanical characterization of lime mortar masonry, a series of finite element analyses was performed in an attempt to assess the capacity of the model to reproduce the results obtained in terms of capacity, failure mode and global stiffness. The constitutive law used for the non-linear analysis of the masonry is a combination of a smeared cracking model in tension and a pressure dependent plasticity model in compression, which is capable of accounting for all failure mechanisms that may arise in concentric compression of masonry, both in the units and in the mortar.

The purpose of this investigation is to establish whether a numerical approach based on the micro-modeling method is suitable for the simulation of the salient features encountered in masonry under compression as well as highlighting the main material properties necessary to be determined in order to properly model such experiments. The results are expanded upon through a parametric investigation.

1. INTRODUCTION

Masonry may be considered a two-phase composite material, composed of units and mortar. Therefore, numerical modeling of masonry structures needs to take into account the accurate geometry of the composite, the behavior of its constituent materials and the nature of their interaction. The detailed micro-modeling approach strives to accomplish this by separately considering the units, the mortar and the unit-mortar interface. Appropriate constitutive laws may be adopted for each component so that the main anticipated characteristics of their behavior can be simulated.

Masonry failure in compression is governed mainly by crushing of the mortar in the horizontal joints and cracking of the units. Furthermore, the units generally have a higher Young's modulus and a lower Poisson's ratio than the mortar. As a result, under vertical loads, the mortar is in triaxial compression and the units under uniaxial compression and biaxial tension. The compressive strength of the composite, for the vast majority of cases, lies

between the compressive strength of the two constituents. Therefore, if a micro-modeling approach is to be adopted, it is necessary, at least in broad terms, to model the pressure dependent behavior of the mortar and the cracking behavior of the units.

Numerical simulation of masonry compression using micro-models and plasticity laws has been performed in the past [1, 2, 3, 4, 8, 11]. These cases involve the simulation of masonry constructed using cement/lime mortar.

In the context of this paper, a set of experimental tests on masonry compression were simulated using micro-modeling techniques and appropriate material laws to model inelastic behavior. The masonry in question was constructed using pure lime mortars. A number of parameters, for which it was not possible to obtain data, were the subject of a parametric investigation.

2. MATERIAL MODEL

2.1 General

The nonlinear behavior of each material is modeled using a total strain concept with secant unloading and a rotating crack assumption. Stress-strain relations are evaluated in the direction of the principal strain vector, which is not fixed at the initiation of damage but may rotate as strains increase.

Six internal damage variables are used to monitor the deterioration of the material in compression and tension. Apart from the reduction of stiffness due to cracking, Poisson effects, meaning the contraction perpendicularly to the direction of crack opening, is reduced. The Poisson's ratio is reduced at the same rate as the Young's modulus [10, 11].

2.2 Behavior in Tension

For the tensile behavior, an exponential softening law based on fracture energy is used. The ultimate crack strain is equal to

$$\varepsilon_u^{cr} = \frac{1}{\alpha}\frac{G_f}{f_t h} \tag{1}$$

where f_t is the tensile strength, G_f is the tensile fracture energy, h is the characteristic element length and α is the total area beneath the softening curve.

2.3 Behavior in Shear

Due to the rotating crack assumption full shear retention may be assumed, meaning that the shear stiffness is not reduced after cracking or, equivalently, that the secant crack shear stiffness is infinite.

2.4 Behavior in Compression

Basic behavior in compression is modeled using a parabolic hardening-softening curve based on fracture energy [7]. The compression curve is defined by the piecewise equation:

$$f = \begin{cases} -f_c \dfrac{1}{3}\dfrac{\varepsilon_j}{\varepsilon_{c/3}} & \text{if } \varepsilon_{c/3} < \varepsilon_j \le 0 \\ -f_c \dfrac{1}{3}\left(1+4\left(\dfrac{\varepsilon_j-\varepsilon_{c/3}}{\varepsilon_c-\varepsilon_{c/3}}\right)-2\left(\dfrac{\varepsilon_j-\varepsilon_{c/3}}{\varepsilon_c-\varepsilon_{c/3}}\right)^2\right) & \text{if } \varepsilon_c < \varepsilon_j \le \varepsilon_{c/3} \\ -f\left(1-\left(\dfrac{\varepsilon_j-\varepsilon_c}{\varepsilon_u-\varepsilon_c}\right)^2\right) & \text{if } \varepsilon_u < \varepsilon_j \le \varepsilon_c \\ 0 & \text{if } \varepsilon_j \le \varepsilon_u \end{cases} \tag{2}$$

where f_c is the compressive strength, $\varepsilon_{c/3}$ is the strain corresponding to one third of the uniaxial strength assuming an elastic stress-strain relation up to that point, ε_c is the strain at which the maximum compressive strength is reached, and is equal to $5\varepsilon_{c/3}$, and ε_u is the peak strain for which it stands:

$$\varepsilon_u = \varepsilon_c - \frac{3}{2}\frac{G_c}{h f_c} \tag{3}$$

where G_c is compressive fracture energy and *h* is the characteristic element length.

The increase in strength and ductility due to isotropic stress is modeled according to the four-parameter Hsieh-Ting-Chen failure surface [9, 10]:

$$f = 2.0108\frac{J_2}{f_{cc}^2} + 0.9714\frac{\sqrt{J_2}}{f_{cc}} + 9.1412\frac{f_{c1}}{f_{cc}} + 0.2312\frac{I_1}{f_{cc}} - 1 = 0 \tag{4}$$

where f_{cc} is the uniaxial compressive strength f_{c1} is the maximum principal stress, and an increase in the peak strain determined by the increase in the peak stress.

Furthermore, the compressive behavior in terms of both peak stress and peak strain is influenced by lateral cracking, which results in a decrease in strength and ductility [12].

3. APPLICATION CASE STUDY

3.1 Experimental Results and Material Properties

An experimental campaign on the compressive behavior of masonry composed of solid clay bricks and pure lime mortar masonry was conducted. The bricks measured 290×140×45 mm^3 and the joints measured 10 *mm* in thickness. 6 masonry stack prism wallettes, 3 of which constructed using aerial lime and 3 using hydraulic lime mortar, were tested in concentric vertical compression. All prisms were composed of five units and four mortar joints. The project included efforts to directly measure, or indirectly determine, the material properties of the constituents and the composite most important for the numerical reproduction of the

experiments.

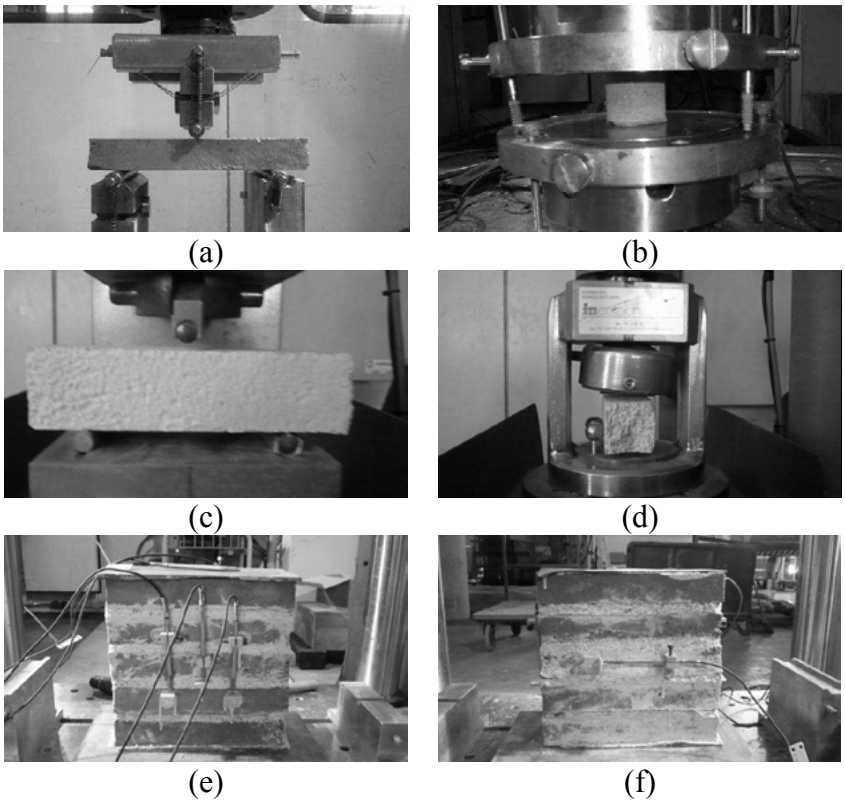

Figure 1: Experimental setups: (a) flexural strength of unit, (b) compressive strength and Young's modulus of unit, (c) flexural strength of mortar, (d) compressive strength of mortar, (e) compressive strength and Young's modulus of masonry, (f) Poisson's ratio of unit.

For the units, the properties measured were the compressive strength, the flexural strength, the Young's modulus perpendicular to the bed face and the Poisson's ratio. For the mortar, the properties measured were the compressive and flexural strength. Finally, for the masonry the compressive strength and the Young's modulus were measured. The small dimensions and very low strength of the mortar samples did not allow for direct measurements to be taken from them with the means and equipment available.

The material properties not measured but necessary for a detailed micro-model include the Young's modulus and Poisson's ratio of the mortar and the tensile and compressive fracture energy of both the units and the mortar.

The tensile strength of both materials was estimated according to the CEB-FIP Model Code 2010 recommendations [6]:

$$f_t = f_{flex}\left(0.06h^{0.7}\right)/\left(1+0.06h^{0.7}\right) \tag{5}$$

where h is the height of the sample tested in bending and f_{flex} is the bending strength.

The tensile fracture energy for all the materials was calculated according to the Model Code 1990 recommendations [5] assuming a 5% ratio of tensile over compressive strength and a maximum aggregate size of 8 *mm*, for which it stands:

$$G_f = 0.025\left(2 f_t\right)^{0.7} \tag{6}$$

The compressive fracture energy for all the materials was calculated assuming a ductility index of 1, where the ductility index is defined as:

$$d = G_C \,/\, f_c \tag{7}$$

The Young's modulus of the mortar was estimated after having acquired the Young's modulus of the units and of the masonry composites. Assuming a distribution of strain according to the uniaxial stiffness of the two components, the mortar and the units, the following expression can be used:

$$E_c = \left(1 + h_m / h_u\right) \Big/ \left(1 + \left(h_m E_u\right) \Big/ \left(h_u E_m\right)\right) E_u \tag{8}$$

The Poisson's ratio of the mortars could not be directly measured, however it has been reported in the literature that the value is not only usually higher than that of the units but that it exhibits rapid increase for an increase in applied vertical compression. Therefore relatively high values of 0.25 were assumed for both the aerial and the hydraulic lime mortar.

Table 1: Unit, mortar and masonry properties.

	$f_{c,u}$ [MPa]	$f_{flex,u}$ [MPa]	$f_{t,u}$ [MPa]	E_u [MPa]	v_u [-]	$G_{c,u}$ [N/mm]	$G_{f,u}$ [N/mm]
Units	23.00	7.29	3.22	4200	0.16	23.00	0.092

	$f_{c,m}$ [MPa]	$f_{flex,m}$ [MPa]	$f_{t,m}$ [MPa]	E_m [MPa]	v_m [-]	$G_{c,m}$ [N/mm]	$G_{f,m}$ [N/mm]
ALM	1.25	0.43	0.19	125	0.25	1.25	0.013
HLM	1.90	0.84	0.37	225	0.25	1.90	0.020

	f_c [MPa]	E_c [MPa]
ALM Masonry	12.03	729
HLM Masonry	13.73	1181

3.2 Modeling and Geometry

As explained in the introduction, each masonry component (unit, or mortar joint) is in a triaxial stress state when subjected to vertical compression. For the purpose of simulating as closely as possible both the geometry and the expected distribution of stress, three dimensional models were used for the numerical reproduction of the experiments. Plane stress and plane strain models may not, therefore, provide accurate descriptions of neither the geometry nor the stress distribution and the development of failure patterns.

The issue of the adequacy of plane methods for this particular problem is addressed in the parametric investigation.

In the finite element models, the units and the mortar were modeled using continuum elements. Twenty-node solid brick elements employing quadratic interpolation and 3×3×3 Gauss integration scheme were used. The bond between two alternating layers was considered perfect: opening of the horizontal unit-mortar interface is impossible in concentric compression and the possibility of shear sliding is countered by the high normal forces.

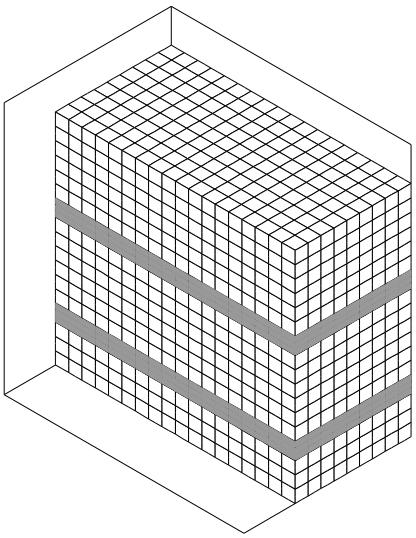

Figure 2: Finite element mesh of masonry prism with symmetry planes indicated.

The loading was applied in displacement control as a uniform vertical displacement of the nodes at the top of the model, using a Modified Newton-Raphson solution method and an energy norm based convergence criterion.

4. RESULTS

4.1 Initial Analysis

The initial numerical results are presented in Table 2. The strength and elastic modulus predicted by the analyses were fairly close to the experimentally derived values. The strength of the ALM masonry was slightly underestimated, that of the HLM masonry was slightly overestimated and the Young's moduli were well within the experimental range.

Table 2: Numerical results from three-dimensional analysis.

	$f_c\,[MPa]$	$E_c\,[MPa]$
ALM Masonry	10.5	814
HLM Masonry	14.8	1287

The failure mode obtained from the numerical analysis closely resembles the one observed in the experiments: mortar crushing, originating from near the surface of the wallette, followed by cracking of the units near the unit-mortar interface and, finally, vertical cracking of the units and complete crushing of the mortar joints. In the analyses, however, the post-peak behavior was far more brittle than the experimentally observed mode, with the stress dropping off to zero soon after the peak (Figure 3). A higher value for the tensile fracture energy of the units could potentially mitigate this phenomenon.

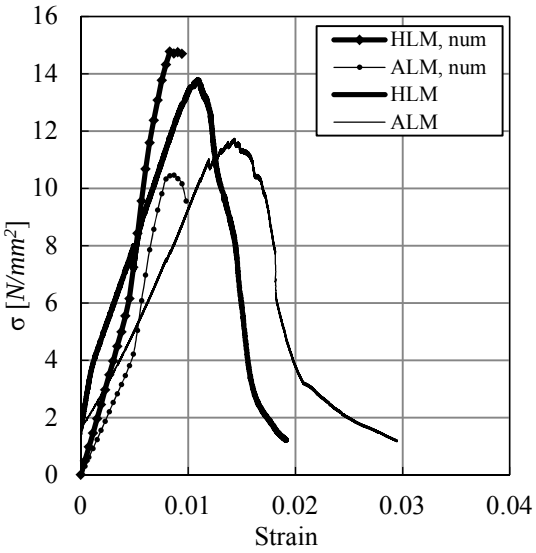

Figure 3: Experimental and numerical stress strain curves.

4.2 Parametric Investigation

The parametric investigation involved the Young's modulus and the Poisson's ratio of the lime mortars. The former property was only indirectly measured while the latter was not measured in the campaign.

The values of the Young's modulus tested extended from half the original experimentally derived values up to 1000 times the compressive strength in *MPa*. The range of values for the Poisson's ratios tested spanned from 0.15 to 0.3.

The results are presented in Table 3, where the influence of the two parameters on the compressive strength and Young's modulus of the masonry is shown. The results are also illustrated in Figure 4.

Table 3: Results of parametric investigation.

	E_m [*MPa*]	vm	f_c [*MPa*]	E_c [*MPa*]		E_m [*MPa*]	vm	f_c [*MPa*]	E_c [*MPa*]
ALM Masonry	65	0.15	4.2	385	HLM Masonry	110	0.15	6.3	662
		0.20	6.8	402			0.20	10.1	689
		0.25	10.4	429			0.25	15.5	731
		0.30	12.8	471			0.30	17.4	797
	125	0.15	4.2	739		225	0.15	6.2	1185
		0.20	6.6	768			0.20	9.7	1225
		0.25	10.5	814			0.25	14.8	1288
		0.30	13.6	885			0.30	17.8	1383
	625	0.15	3.7	2296		950	0.15	5.5	3131
		0.20	5.6	2342			0.20	8.2	2894
		0.25	8.5	2413			0.25	12.4	2928
		0.30	11.0	2519			0.30	16.0	3009
	1250	0.15	3.5	3126		1900	0.15	5.1	3660
		0.20	5.0	3157			0.20	6.9	3598
		0.25	7.2	3208			0.25	9.7	3627
		0.30	9.4	3285			0.30	12.1	3676

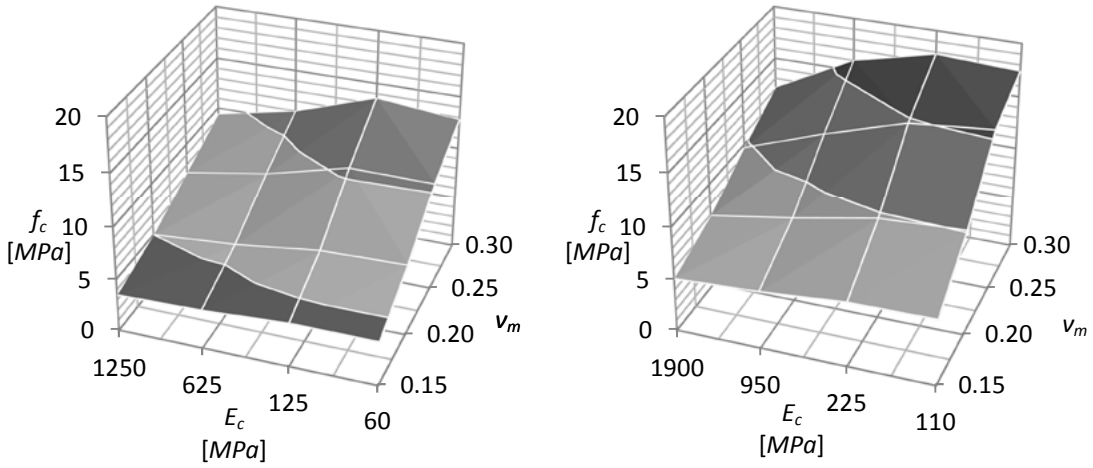

Figure 4: Influence of E_m and v_m on masonry compressive strength: (a) ALM, (b) HLM.

In general, increasing the Poisson's ratio causes the compressive strength of masonry to increase as well. The phenomenon is more pronounced when a low value for the Young's modulus of the mortar is assumed. Similarly, a lower Young's modulus results in a higher obtained compressive strength.

Altering the Poisson's ratio of the mortar also affects the global stiffness of the masonry. The greater the difference between the Poisson's ratios of the units and the mortar the greater the increase in the elastic stiffness of the composite.

4.3 Three Dimensional vs. Plane Models

The adequacy of plane stress and plane strain to model the masonry composite in compression may be evaluated by comparing the obtained strength, Young's modulus and failure mode from each method. A comparison between the results from all geometrical assumptions tested is presented in Table 4.

Table 4: Numerical results from plane stress (PS), three-dimensional (3D) and plane strain (PE) analyses.

		f_c [MPa]	E_c [MPa]
ALM Masonry	PS	1.49	746
	3D	10.46	814
	PE	11.76	825
HLM Masonry	PS	2.22	1197
	3D	14.77	1287
	PE	15.77	1310

The compressive strength and the failure mode obtained differ distinctly. Compared with the experimental results, plane stress results in a marked underestimation of the compressive strength and plane strain leads to a slight overestimation.

In the plane stress models the mortar joints yielded in its entirety, while only a few cracks were registered near the unit mortar-interface. Plane strain results in a mixed failure mode of

mortar yielding in compression and unit cracking, the latter being slightly more pronounced than in the three-dimensional model.

Plane stress neglects the out-off-plane confinement the units afford on the mortar while plane strain may exaggerate it. In the case of masonry composed of very weak mortar, such as the ones studied here, where the failure of the mortar strongly influences the overall behavior of the masonry, plane stress becomes inaccurate. Plane strain is of comparable accuracy to the three dimensional model since, due to the large differences in the elastic properties between the units and the mortar, the confinement of the mortar is strong.

Initial stiffness is also different across the modeling methods, but less so than the compressive strength. Plane strain had the highest Young's modulus, followed by the three-dimensional model and the plane stress model.

5. CONCLUSIONS

Good agreement was found between the values of compressive strength obtained from the experiments and their simulation using the combined plasticity-cracking law. The elastic moduli were also well approximated, within the experimental range but slightly above the experimental average. The failure mode that initiates collapse is captured by the model.

Numerical simulation of masonry in compression using three-dimensional micro-models, while requiring detailed knowledge of the mechanical properties of the materials and the composite, can lead to satisfactory results.

The influence of the Poisson's ratio of the mortar on the compressive strength of masonry is strong when soft mortars and relatively strong units are used. The influence of the Young's modulus of the units is also notable.

ACKNOWLEDGMENTS

This research has received the financial support from the *Ministerio de Economia y Competitividad* through the research projects SUBTIS (*Study of the Sensitivity of Urban Buildings to Tunneling Induced Settlements*, ref. num. BIA2009-13233) and the research project MICROPAR (*Identification of mechanical and strength parameter of structural masonry by experimental methods and numerical micro-modelling*, ref num. BIA2012-32234) and from the ERDF (*European Regional Development Fund*).

REFERENCES

[1] J.M. Adam, A. Brencich, T.G. Hughes, T. Jefferson, Micromodelling of eccentrically loaded brickwork: Study of masonry wallettes, *Engineering Structures* (2010) **32**:1244:1251.

[2] A. Akbarzade, A. Tasnimi, Nonlinear Analysis and Modeling of Unreinforced Masonry Shear Walls Based on Plastic Damage Model, *Journal of Seismology and Earthquake Engineering* (2011) **11**:8:12.

[3] C.S. Barbosa, P.B. Lourenço, J.B. Hanai, On the compressive strength prediction for concrete masonry prisms, *Materials and Structures* (2009) **43**:331:344.

[4] A. Brencich, C. Corradi, L. Gambarotta, Compressive strength of solid clay brick masonry under eccentric loading, in: *Proceedings British Masonry Society*, (2002).

[5] CEB-FIP, *Model Code 1990*, Thomas Telford (1993).

[6] CEB-FIP, *Model Code 2010*, Thomas Telford (2012).

[7] P.H. Feenstra, Computational Aspects of Biaxial Stress in Plain and Reinforced Concrete, PhD dissertation, Delft University of Technology, Delft, The Netherlands, 1993.
[8] T. Furtmüller, C. Adam, Numerical modeling of the in-plane behavior of historical brick masonry walls, *Acta Mechanica* (2011) **221**:65:77.
[9] S.S. Hsieh, E.C. Ting, W.F. Chen, A plastic-fracture model for concrete, *International Journal of Solids and Structures* (1982) **18**:181:197.
[10] R.G. Selby, F.J. Vecchio, Three-dimensional Constitutive Relations for Reinforced Concrete, University of Toronto, Department of Civil Engineering (1993).
[11] C. V. Uday Vyas, B. V. Venkatarama Reddy, Prediction of solid block masonry prism compressive strength using FE model, *Materials and Structures* (2009) **43**:719:735.
[12] F.J. Vecchio, M.P. Collins, The modified compression-field theory for reinforced concrete elements subjected to shear, *American Concrete Institute Journal* (1986) **83**:219:231.